Review

A Mystery in Thermoelectric Layered Cobaltites; the Correlation between Magnetism and Transport Properties on the Two-Dimensional Triangular Lattice

Jun Sugiyama

コバルト酸化物熱電体の不思議：2次元3角格子における磁性と電子輸送現象の相関

杉山純

Abstract

Using muon spin spectroscopy we have found that, for both Na_xCoO_2 ($0.6 \leq x \leq 0.9$) and 3- and 4-layer cobaltites, a common low temperature magnetic state (which in some cases is manifest as an incommensurate spin density wave) forms in the CoO_2 planes. Here we summarize those results and report an almost dome-shaped relation between the transition temperature into the low-T magnetic state and the composition x for Na_xCoO_2 and/or the high-temperature asymptotic limit of thermopower in the more complex 3- and 4-layer cobaltites. This behavior is explained using the Hubbard model on two-dimensional triangular lattice in the CoO_2 plane.

Keywords: Muon spin rotation/relaxation, Spin density wave, Thermoelectrics, Cobaltites, Two-dimensional triangular lattice

要　旨

良好な熱電性能を示す一連の層状コバルト酸化物の磁性を，ミュオンスピン回転・緩和法により調べた。最も単純な構造のNa_xCoO_2のみならず3重あるいは4重岩塩層を含む全ての層状コバルト酸化物で，低温でほぼ同様の磁性相がCoO_2面に形成されることを見出した (この磁性相の構造は多くの場合，非整合スピン密度波状態だった)。ここではこれらの測定結果をまとめ，転移温度とCoO_2面のCo価数との間に共通のドーム型の関係があることを示す。この挙動は，スピンが半充填近傍にある2次元3角格子 (つまりCoO_2面) へハバード模型を適用することにより統一的に説明された。

キーワード：ミュオンスピン回転・緩和，スピン密度波，熱電体，コバルト酸化物，2次元3角格子

1. Introduction

Although the widespread current interest in the layered cobaltites (*i.e.*, 5 K superconductivity in $Na_{0.35}CoO_2{*}2H_2O$)[1, 2] was originally due mainly to their unique combination of high thermopower *S* with metallic transport properties,[3–10] which makes them one of the most promising systems for power applications, we have shown that they also display interesting and complex magnetic orderings, directly correlated with the enhanced *S*. The richness of behavior of the layered cobaltites is due to their intrinsic structure, namely: electrically active triangular planes of CoO_2, which are separated by a variety of intermediate structures; their relatively strong electronic correlations; and the fact that the structures between the CoO_2 planes can be modified in a variety of ways to vary their dimensionality, ionic states, carrier doping in the CoO_2 planes and the relevant interaction strengths.

At present, the following three groups of cobaltites are known to be good thermoelectrics, because they display metallic conductivities as well as high thermoelectric powers *S*, for reasons which are currently not fully understood.

1. : $Na_x[CoO_2]$,[3–5]
2. : $[Ca_2CoO_3]^{RS}_{0.62}[CoO_2]$,[6–8]
3. : $[Sr_2Bi_2O_4]^{RS}_{0.5}[CoO_2]$.[9, 10]

Here, RS stands for a rocksalt-type block; a triple rocksalt-type block for the group No. 2 and a quadruple group for No. 3. All share a common structural component, the CoO_2 planes, in which a two-dimensional triangular lattice of Co ions is formed by a network of edge-sharing CoO_6 octahedra (see **Fig. 1**). Charge carrier transport in these cobaltites is thought to be restricted mainly to the CoO_2 planes, as in the case of the CuO_2 planes for the high-T_c cuprates. Since specific heat measurements on Na_xCoO_2 indicate a large thermal effective mass of carriers,[11] all these cobaltites are believed to be strongly correlated electron systems.

In order to elucidate the magnetism in the CoO_2 planes and the mechanism of the good thermoelectric properties, we have carried out positive muon spin rotation and relaxation (μ^+SR) experiments on the layered cobaltites. As a result, we found the transition from a high-temperature paramagnetic to a low-*T* commensurate or incommensurate spin density wave (C- or IC-SDW) state for $[Ca_2CoO_3]^{RS}_{0.62}[CoO_2]$ below ~100 K,[12, 13] $Na_{0.75}CoO_2$ at 22 K[14] and $[Ca_2Co_{4/3}Cu_{2/3}O_4]^{RS}_{0.62}[CoO_2]$ below ~200 K.[15] The common magnetic ordering is thus not always that of a classic frustrated AF (triangular planar arrangement of spins) system but rather a variety of states including disordered AF and (most common) an IC-SDW, arising in parallel with other effects in the triangular lattice such as effective mass enhancement and the enhanced *S* in the Na_xCoO_2 case. The more complex cobaltites exhibit, in addition, other magnetic orderings and even higher *S*.

Nevertheless, the transition temperature was scattered in the wide *T* range (22 - 200 K), and there was no clear relationship between T_{SDW} and structural properties and/or carrier concentration of the layered cobaltites. We back therefore to the basic system, Na_xCoO_2, to investigate the dependence of T_{SDW} on *x* by μ^+SR. Also, for the multilayer systems, we clarify the magnitude of T_{SDW} as a function of the Co valence varied by the change in composition of the rocksalt-type subsystem.[16–18] For the Na_xCoO_2 case, we show that a calculation based on the Hubbard model for a triangular lattice of **S** =1/2 Co ions with occupancy given by *x* (correlated with band filling)[19–21] is able to explain the dome shaped magnetic phase diagram

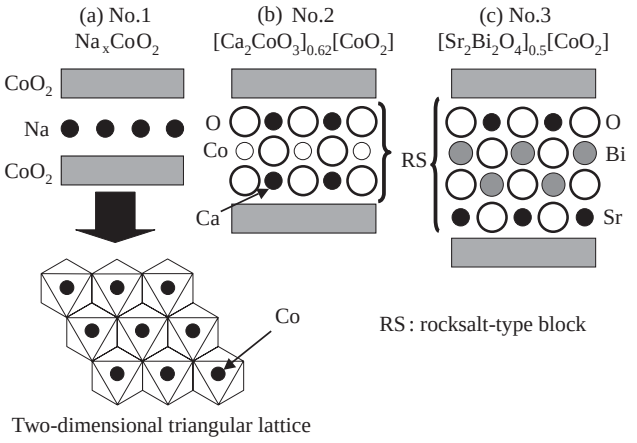

Fig. 1 Schematic crystal structures of layered cobaltites; (a) Na_xCoO_2, (b) 3-layer cobaltites, and (c) 4-layer cobaltites.

shown below.[22, 23] Similar behavior is observed for the multilayer systems, where the increased two dimensionality due to the extra layers leads to higher T_{SDW} and is correlated with higher S.

2. Experiment

2. 1 μ^+SR

Muon spin rotation and relaxation (μSR) is an important tool for probing local static and dynamic magnetic properties, especially for detecting magnetic order/ disorder and determining a magnetic phase diagram in magnetic materials.[24, 25] Actually, the magnetic phase diagram of the superconducting cuprates were clarified by μSR experiments.[26]

Since μSR requires low energy muons in order to stop the beam in samples of convenient thickness (below 1 cm), the required intensities are available only from ordinary two-body pion π decay, from which the muon emerges (in the rest frame of the pion) with a momentum of 29.79 MeV/c and a kinetic energy of 4.119 MeV(*i.e.*, surface muon). The lifetime of a free charged pion is 26.03 ns.

$$\pi^+ \longrightarrow \mu^+ + \nu_\mu , \quad \cdots\cdots\cdots\cdots\cdots\cdots (1)$$

where ν_μ is muon neutrino and pions in turn are produced in medium energy nucleon-nucleon collisions as,

$$p + p \longrightarrow \pi^+ + p + n. \quad \cdots\cdots\cdots\cdots\cdots\cdots (2)$$

Typically, one directs a beam of proton p with a kinetic energy in the range 0.5-1 GeV onto a target of light nuclei such as Be or C.

The most remarkable feature of positive π decay is that it maximally violates Parity symmetry, causing the μ to be emitted with perfect spin polarization. This is the greatest advantage of μSR as a magnetic resonance technique: whereas NMR and ESR rely upon a thermal equilibrium spin polarization, usually achieved at low temperatures in strong magnetic fields, μSR begins with a perfectly polarized probe, regardless of conditions in the medium to be studied. It also implies that muon spin degrees of freedom usually start their evolution as far from thermal equilibrium as conceivable.

Once the muons are implanted within a sample and stopped usually at interstitial sites much less than 1 nsec, their local magnetic environment dictates the subsequent evolution of their spin vectors. If the muons experience a unique off-axis magnetic field (either internal or applied), the spins precess coherently around the filed at their Larmor frequency. However any spatial or temporal, site to site, variation of the magnetic field results in dephasing or depolarization of the muon spin ensemble. This precessional motion and/or depolarization of the muon spins can be monitored because of the propensity of the muon decay positron e^+ to be emitted preferentially along the spin direction of muon, a further consequence of Parity-violation in the weak interaction. In a μSR experiment, the information on the distribution of local magnetic environments over all muon sites is thus delivered to the observer in the form of relatively high energy (up to 53 MeV) decay e^+ which readily penetrate sample holders, cryostats or ovens and the detectors used to establish the time and direction of the muon spin at the instant decay.

$$\mu^+ \longrightarrow e^+ + \nu_e + \nu_\mu , \quad \cdots\cdots\cdots\cdots\cdots\cdots (3)$$

Currently, there are only four pion/muon factories in the world; that is, TRIUMF at Vancouver in Canada, PSI in Switzerland, ISIS at Rutherford Appleton Laboratory in UK and KEK in Japan. The former two factories are continuous sources suitable for the observation of rapid muon spin rotation and relaxation, whereas the latter two pulsed facilities for slow relaxation. The μ^+SR experiments reported here were performed on the **M15** and **M20** surface muon beam lines at TRIUMF. The experimental setup and techniques were described in detail in elsewhere.[24, 25]

Here, we have measured both weak (~100 Oe) transverse-field positive muon spin rotation and relaxation (wTF-μ^+SR) and zero field (ZF-) μ^+SR time spectra. The former method is sensitive to local magnetic order *via* the shift of the μ^+ spin precession frequency and the enhanced μ^+ spin relaxation, while ZF-μ^+SR is sensitive to weak local magnetic [dis]order in samples exhibiting quasi-static paramagnetic moments.

2. 2 Sample preparation

Single-crystal platelets of Na_xCoO_2 were prepared by a flux method.[27] Polycrystalline $Na_{0.75}CoO_2$ and $Na_{0.65}CoO_2$ were synthesized by a modified solid state reaction technique, *i.e.*, a "rapid heat-up" technique.[28] Polycrystalline 3- and 4-layer cobaltites listed in **Table 1** (see p.10) were synthesized by a

solid state reaction technique[12, 16–18] or a reactive templated grain growth technique.[29, 30]

3. Results

3. 1 Na_xCoO_2[14, 22, 23]

Polycrystalline $Na_{0.75}CoO_2$ exhibited a magnetic transition at 22 K accompanying the increase in the slope of the resistivity-*vs*.-*T* ($\rho(T)$) curve and the appearance of the large positive magnetoresistance effect, while no transitions were found in $Na_{0.65}CoO_2$ down to 2 K.[31] Interestingly, both ρ^{-1} and *S* of $Na_{0.75}CoO_2$ were significantly larger than those of $Na_{0.65}CoO_2$.[28] In other words, the thermoelectric properties of Na_xCoO_2 seem to be enhanced by the magnetic interaction between 3*d* electrons which induces the magnetic transition. On the other hand, $Na_{0.9}CoO_2$ was reported to exhibit a magnetic transition at 19 K, although ρ (300 K) in $Na_{0.9}CoO_2$ was higher by one order of magnitude than that of $Na_{0.6}CoO_2$.[27] Therefore, to investigate the magnetism of Na_xCoO_2 in greater detail, we have measured μ^+SR spectra in Na_xCoO_2 with x = 0.6 - 0.9 at temperatures below 300 K.

Figure 2 shows zero-field (ZF-)μ^+SR time spectra at 1.8 K for single crystal platelets of $Na_{0.9}CoO_2$. The top spectrum was obtained with the initial μ^+ spin direction $\boldsymbol{S}_\mu(0)$ perpendicular to the *c*-axis and the bottom one with $\boldsymbol{S}_\mu(0)$ parallel to $\boldsymbol{c}$. A clear oscillation due to quasistatic internal fields is observed only for the $\boldsymbol{S}_\mu(0) \perp \boldsymbol{c}$ case. The oscillation in the top spectrum is characteristic of a zeroth-order Bessel function of the first kind $J_0(\omega_\mu t)$ that describes the muon polarization evolution in an IC-SDW field distribution.[24, 32] Actually, the top oscillating spectrum was fitted using a combination of three signals:

$$A_0 P(t) = A_{SDW} J_0(\omega_\mu t) \exp(-\lambda_{SDW} t)^{\beta_{SDW}} + A_{KT} G_{ZZ}^{KT}(t, \Delta) + A_x \exp(-\lambda_x t)^{\beta_x}, \quad \cdots\cdots\cdots (4)$$

$$\omega_\mu \equiv 2\pi f_\mu = \gamma_\mu \boldsymbol{H}_{int}, \quad \cdots\cdots\cdots\cdots\cdots (5)$$

$$G_{ZZ}^{KT}(t, \Delta) = 1/3 + 2/3\,(1-\Delta^2 t^2) \exp(-\Delta^2 t^2/2), \quad \cdots\cdots\cdots\cdots\cdots (6)$$

where A_0 is the empirical maximum muon decay asymmetry, A_{SDW}, A_{KT} and A_x are the asymmetries associated with the three signals, $G_{ZZ}^{KT}(t, \Delta)$ is the static Gaussian Kubo-Toyabe function, Δ is the static width of the distribution of local frequencies at the disordered sites, λ_x is the slow relaxation rate and β_{SDW} and β_x are the power of the exponential relaxation. Fits using just an exponentially damped cosine oscillation, $\exp(-\lambda t)\cos(\omega_\mu t + \phi)$, provides a phase angle $\phi \sim -42^\circ$, which is physically meaningless.[24]

We therefore conclude that $Na_{0.9}CoO_2$ undergoes a transition from a paramagnetic to an IC-SDW state at T_{SDW} =19 K. The absence of a clear oscillation for the $\boldsymbol{S}_\mu(0) \parallel \boldsymbol{c}$ case indicates that the internal field $\boldsymbol{H}_{int}$ is roughly parallel to the *c*-axis. Due to the strong anisotropy, the IC-SDW is thus considered to localize in the CoO_2 plane, with oscillating moments directed along the *c*-axis, as in the case of $[Ca_2CoO_3]^{RS}_{0.62}[CoO_2]$.[14] Moreover, this anisotropic result is consistent with χ measurements. That is, the cusp at 19 K was observed, when $\boldsymbol{H}$ was applied parallel to the *c*-axis, whereas the cusp was undetected if $\boldsymbol{H} \perp \boldsymbol{c}$.[27]

Figure 3 shows the *T* dependence of the muon precession frequency $f_\mu = \omega_\mu/2\pi$ for the single crystal platelets of $Na_{0.9}CoO_2$. Here f_μ is the order parameter of the transition and its *T* dependence is well described by the BCS weak coupling expression for such order parameters, as expected for the IC-SDW state.[33] The magnetic phase diagram (**Fig. 4**) of Na_xCoO_2 can thus be sketched

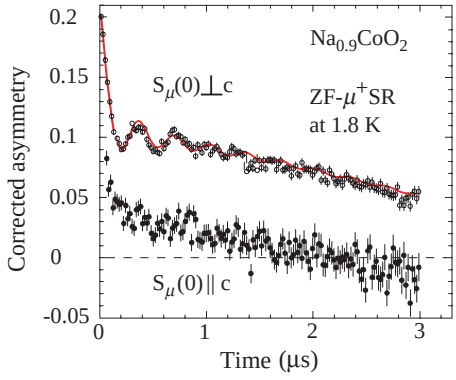

Fig. 2 ZF-μ^+SR time spectra of single crystal platelets of $Na_{0.9}CoO_2$ at 1.8 K. The configurations of the sample and the initial muon spin direction $\boldsymbol{S}_\mu(0)$ are (top) $\boldsymbol{S}_\mu(0) \perp \boldsymbol{c}$ and (bottom) $\boldsymbol{S}_\mu(0) \parallel \boldsymbol{c}$. The bottom spectrum is offset below to be seen clearly.

from the μ^+SR results for polycrystalline samples with x = 0.65 and 0.75[14] and the present x = 0.6 and 0.9 crystals. According to recent compositional and chemical titration analyses, the oxygen deficiency δ in $Na_xCoO_{2-\delta}$ is negligibly small even for the x = 0.9 sample.[27] Hence, the average Co valence is directly calculated from x. As x increases from 0.6 (*i.e.* the Co valence decreases from 3.4), the magnitude of T_{SDW} increases up to around x = 0.8, then decreases with further increasing x. As a result, we obtain the dome-shaped relationship of Fig. 4 between T_{SDW} and x, *viz.* the Co valence for Na_xCoO_2.

Although a fully occupied Na_xCoO_2 phase cannot be prepared by conventional solid state reaction and/or flux techniques, the related compound $LiCoO_2$ is easily obtained. The structure of $LiCoO_2$ is almost the same as that of Na_xCoO_2, and it is reported to be diamagnetic down to 4.2 K,[34] indicating the Co^{3+} in $LiCoO_2$ are in a low-spin state t_{2g}^6, as for Na_xCoO_2. Therefore, Na_xCoO_2 is also expected to lack magnetically ordered states.

The occupancy of Co^{4+} spins (**S** = 1/2) in the two-dimensional triangular lattice (2DTL) increases with decreasing x. A fully Na deficient Na_0CoO_2 would be a half filled 2DTL; that is, every lattice site is occupied by an **S** = 1/2 spin. The Hubbard model within a mean field approximation can be used for explaining the magnetism of such a system, with the Hamiltonian H.[19-21]

$$H = -t\sum_{<ij>\sigma} c_{i\sigma}^{\dagger} c_{j\sigma} + U\sum_{i} n_{i\uparrow} n_{i\downarrow}, \quad \cdots\cdots\cdots (7)$$

where $c_{i\sigma}^{\dagger}$ ($c_{j\sigma}$) creates (destroys) an electron with spin σ on site i, $n_{i\sigma} = c_{i\sigma}^{\dagger} c_{i\sigma}$ is the number operator, t is the nearest-neighbor hopping amplitude and U is the Hubbard on-site repulsion. The electron filling n is defined as $n = (1/2N)\sum_i^N n_i$, where N is the total number of sites.

At T = 0 and n = 0.5 (*i.e.*, Na_0CoO_2), as U increases from 0, the system is a paramagnetic (PM) metal up to U/t = 3.97 due to geometrical frustration, then changes into a metal with a spiral IC-SDW, and then at U/t = 5.27 a first-order metal-insulator transition occurs.[19] The lack of magnetic transitions for Na_xCoO_2 with x = 0.6 and 0.65 suggests that $U/t \leq$ 3.97. This means that Na_xCoO_2 is unlikely to be a typical strongly correlated electron system, because $U \gg t$ for such a system. The calculations[20] also predict that, as n increases from 0, the value of U/t at the boundary between the PM and SDW phases decreases, with increasing slope ($d(U/t)/dn$) up to n = 0.75. Even for U/t = 0, the SDW phase is stable at n = 0.75. The value of U/t then increases with further increasing n, with decreasing slope. Therefore, the dome-shaped phase diagram of Fig. 4 is qualitatively explained by the calculations, although the measured maximum of the dome is located around x = 0.8 (*i.e.* n = 0.9). This is likely due to the simple band structure assumed in the above calculation, while calculations for Na_xCoO_2

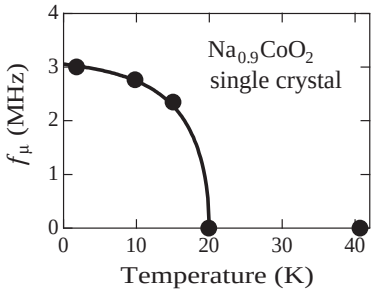

Fig. 3 Temperature dependence of the muon precession frequency f_μ in $Na_{0.9}CoO_2$. The solid line represents the temperature dependence of the BCS gap energy.

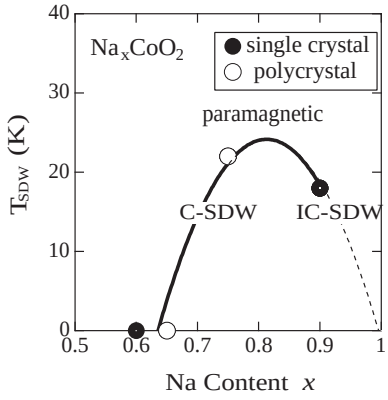

Fig. 4 Phase diagram of Na_xCoO_2 determined by the μ^+SR experiments. Solid and open circles represent the present results on single crystals and polycrystalline samples, respectively. The point at x =1 is extrapolated from the data on the related compound $LiCoO_2$.[34]

suggest more complicated one.[35)]

3. 2 $[Ca_2CoO_3]_{0.62}[CoO_2]$[12, 13)] and $[Ca_2Co_{4/3}Cu_{2/3}O_3]_{0.62}[CoO_2]$[15)]

The crystal structure of $[Ca_2CoO_3]^{RS}_{0.62}[CoO_2]$ consists of alternating layers of the triple rocksalt-type $[Ca_2CoO_3]$ subsystem and the single CdI_2-type $[CoO_2]$ subsystem stacked along the *c*-axis.[7, 8)] There is a misfit between these subsystems along the *b*-axis. Susceptibility (χ) measurements[7, 12)] indicate two magnetic transitions at 19 K and 380 K; the former is a ferrimagnetic transition (T_{FR}) and the latter is probably a spin-state transition (T^{χ}_{SS}). The temperature dependence of the resistivity ρ exhibits a broad minimum around 80 K[7, 8, 12)] and a broad maximum between 400 and 600 K.[7)] Although ρ appears to diverge with decreasing temperature below T_{FR}, it is worth noting that $\chi(T)$ shows no clear anomalies near 80 K or 600 K.

In all the $[Ca_2CoO_3]^{RS}_{0.62}[CoO_2]$ samples, the wTF-μ^+SR spectra in a magnetic field of H ~100 Oe exhibit a clear reduction of the μ^+ precession amplitude below 100 K. The data were obtained by fitting the wTF-μ^+SR spectrum in the time domain with a combination of a slowly relaxing precessing signal and two non-oscillatory signals, one fast and the other slow relaxing:

$$A_0 P(t) = A_{para} \exp(-\lambda_{para} t) \cos(\omega_\mu t + \phi) + A_{fast} \exp(-\lambda_{fast} t) + A_{slow} \exp(-\lambda_{slow} t), \quad \cdots\cdots\cdots\cdots (8)$$

where ω_μ is the muon Larmor frequency, ϕ is the initial phase of the precession and A_n and λ_n (n = para, fast and slow) are the asymmetries and exponential relaxation rates of the three signals. The latter two signals (n = fast and slow) have finite amplitudes below $T^{on}_{SDW} \approx 100$ K and probably suggest the existence of multiple muon sites in $[Ca_2CoO_3]^{RS}_{0.62}[CoO_2]$.

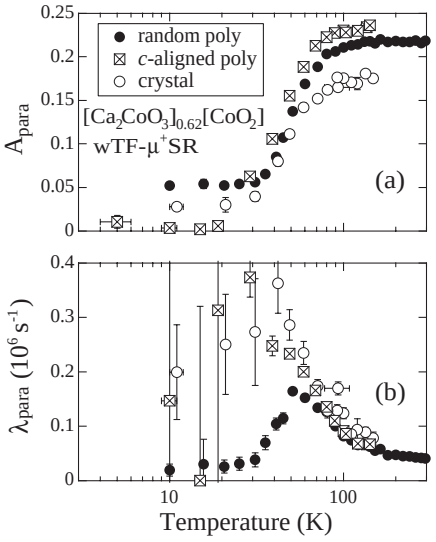

Fig. 5 (a) Paramagnetic μ^+ spin precession asymmetry A_{para} and (b) muon spin relaxation rate λ_{para} as a function of temperature for the three $[Ca_2CoO_3]^{RS}_{0.62}[CoO_2]$ samples: a randomly oriented polycrystalline disk (solid circles),[12)] a *c*-axis aligned polycrystalline plate (squares) and single crystal (sc) platelets (open circles). For the sc platelets, both the value of A_{para} above 100 K and the change in A_{para} below 100 K are smaller than those in the polycrystalline samples. This is because the muon momentum was decreased from 28 to 25 MeV/c for the sc measurements to stop muons in the thin platelets (~100 μm thickness), causing a small background signal from muons stopping elsewhere.

Figures 5(a)-(b) show the temperature dependences of the paramagnetic asymmetry A_{para} (which is proportional to the volume fraction of a paramagnetic phase in the sample) and the corresponding relaxation rate λ_{para} in three $[Ca_2CoO_3]^{RS}_{0.62}[CoO_2]$ samples: a randomly oriented polycrystalline sample,[12)] a *c*-aligned polycrystalline sample, and single crystal platelets. The large decrease in A_{para} below 100 K (and the accompanying increase in λ_{para}) indicate the existence of a magnetic transition with an onset temperature $T^{on}_c \approx 100$ K and a transition width $\Delta T \approx 70$ K. The single crystal data suggest that the large ΔT is not caused by inhomogeneity of the sample but is an intrinsic property of this compound. **Figure 6** shows ZF-μ^+SR time spectra at 4.8 K in the *c*-aligned sample; the top spectrum was obtained with the initial μ^+ spin direction $\boldsymbol{S}_\mu(0)$ perpendicular to the *c*-axis and the bottom one with $\boldsymbol{S}_\mu(0) \parallel \boldsymbol{c}$. A clear oscillation due to quasi-static internal fields is observed only when $\boldsymbol{S}_\mu(0) \perp \boldsymbol{c}$. The top oscillating spectrum is a characteristic of $J_0(\omega_\mu t)$ that describes the muon polarization evolution in an IC-SDW field distribution,[24, 32)] and was fitted using a combination of three signals, as in the case of $Na_{0.9}CoO_2$:

$$A_0 P(t) = A_{SDW} J_0(\omega_\mu t) \exp(-\lambda_{SDW} t) + A_{KT} G^{KT}_{ZZ}(t, \Delta) + A_{tail} \exp(-\lambda_{tail} t), \quad \cdots\cdots\cdots\cdots (9)$$

where A_{SDW}, A_{KT} and A_{tail} are the asymmetries associated with the three signals and λ_{tail} is the slow relaxation rate of the "tail" (not shown in this Figure).

We therefore conclude that $[Ca_2CoO_3]^{RS}_{0.62}[CoO_2]$ undergoes a magnetic transition from a paramagnetic state to an IC-SDW state (*i.e.* $T_c^{on} = T_{SDW}^{on}$). The absence of a clear oscillation in the bottom spectrum of Fig. 6 indicates that the internal magnetic field $\boldsymbol{H}_{int}$ is roughly parallel to the *c*-axis, since the muon spins do not precess in a parallel magnetic field. The IC-SDW is unlikely to propagate along the *c*-axis due both to the two-dimensionality and to the misfit between the two subsystems. The IC-SDW is therefore considered to propagate in the *a*-*b* plane, with oscillating moments directed along the *c*-axis. This suggests that the ferrimagnetic interaction is also parallel to the *c*-axis, and is consistent with the results of our χ measurement on single crystals.[36)]

Figures 7(a)-(b) show the temperature dependences of A_{SDW}, A_{KT} and A_{para} (same in Fig. 5), f_μ and λ_{SDW} and Δ for the *c*-aligned $[Ca_2CoO_3]^{RS}_{0.62}[CoO_2]$. A_{SDW} increases with decreasing T below 30 K, although A_{para} obtained by the wTF-μ^+SR measurement exhibits a rapid decrease below 100 K and levels off to almost 0 below 30 K (see Fig. 7(a)). According to the recent χ measurements using single crystal platelets,[36)] a small shoulder in the $\chi(T)$ curve was observed at 27 K only for $\boldsymbol{H} \perp \boldsymbol{ab}$. This temperature (27 K) corresponds to the highest temperature that a clear μ^+SR signal due to the IC-SDW was observed. Thus, it is considered that a short range order IC-SDW state appears below 100 K = T_{SDW}^{on}, while the long-range order is completed below 27 K; *i.e.*, $T_{SDW} = T_{SDW}^{end}$. Since both $\rho(T)$ and $S(T)$ are metallic above 80 K and semiconducting below 80 K,[7, 8)] charge carrier transport is strongly affected by a formation of the short-range IC-SDW order.

Although the $f_\mu(T)$ curve is well explained by the BCS weak coupling theory as expected for the IC-SDW state,[33)] there is a deviation from the theory around 20 K (see Fig. 7(b)). This deviation (and the accompanying increase in A_{SDW}) is probably due to the effect of the ferrimagnetic transition at 19 K (= T_{FR}). Here, the ferrimagnetism is considered to be caused by an interlayer coupling between Co spins in the $[Ca_2CoO_3]$ and $[CoO_2]$ subsystems,[36)] while the IC-SDW order completes below 27 K. This means that the IC-SDW is affected by the ferrimagnetic coupling *via*. the Co spins in the $[Ca_2CoO_3]$ subsystem. Therefore, the enhancement of the internal magnetic field at T_{FR} is likely to be

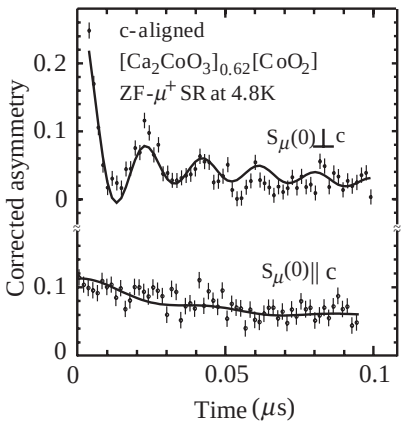

Fig. 6 ZF-μ^+SR time spectra of the *c*-aligned $[Ca_2CoO_3]^{RS}_{0.62}[CoO_2]$ plate at 4.8 K. The configurations of the sample and the initial muon spin direction $\boldsymbol{S}_\mu(0)$ are (top) $\boldsymbol{S}_\mu(0) \perp \boldsymbol{c}$ and (bottom) $\boldsymbol{S}_\mu(0) \parallel \boldsymbol{c}$.

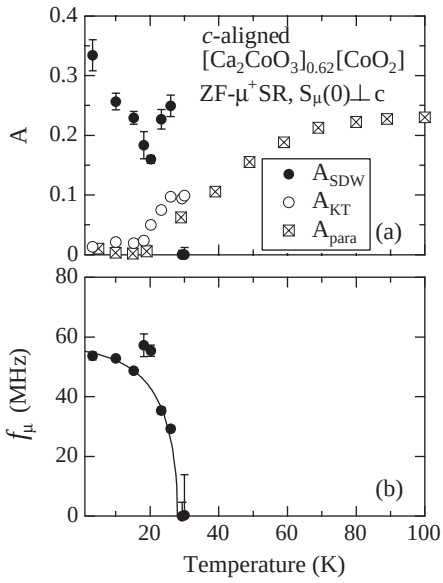

Fig. 7 Temperature dependences of (a) A_{SDW} and A_{para} (estimated by the wTF-μ^+SR experiment) and (b) f_μ for the *c*-aligned $[Ca_2CoO_3]^{RS}_{0.62}[CoO_2]$. The solid line in Fig. 7(b) represents the temperature dependence of the BCS gap energy. The deviation of the experimental data from the theory around 20 K is probably due to the effect of the ferrimagnetic transition at 19 K.

caused by a critical phenomenon around the ferrimagnetic transition. In addition, the magnitude of λ_{SDW} decreases rapidly with decreasing T and levels off to a constant value below 20 K. This suggests that the broadening of the IC-SDW field distribution at the μ^+ sites mainly occurs in the temperature range between T_{SDW} and T_{FR}.

In order to determine the subsystem in which the IC-SDW exists, ZF-μ^+SR spectra were measured in doped samples: *c*-aligned polycrystalline $[Ca_{1.8}M_{0.2}CoO_3]^{RS}_{0.62}[CoO_2]$ (M = Sr, Y and Bi). A clear precession was observed in the ZF-μ^+SR spectrum with $\boldsymbol{S}_{\mu}(0) \perp \boldsymbol{c}$ in every sample, although T_{SDW} depended on dopant. **Figure 8** shows the temperature dependences of f_μ for the *c*-aligned pure and doped $[Ca_2CoO_3]^{RS}_{0.62}[CoO_2]$ samples. Doping with Y and Bi increase T_{SDW} by ~40 K and Sr-doping by ~20 K, although Sr-doping did not affect T^{on}_{SDW} by the previous wTF-μ^+SR experiment.[12)]

It should be noted that all the samples show approximately the same precession frequency (~60 MHz) at zero temperature. This suggests that the local magnetic field $\boldsymbol{H}_{int}(0\ \mathrm{K})$ is independent of dopant. Since $\boldsymbol{H}_{int}$ in the doped $[Ca_2CoO_3]$ subsystem should be strongly affected by the dopant, it is concluded that the IC-SDW exists not in the $[Ca_2CoO_3]$ subsystem but in the $[CoO_2]$ subsystem.

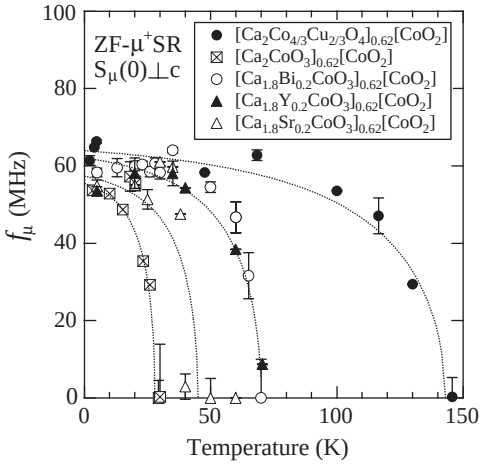

Fig. 8 Temperature dependences of f_μ for the *c*-aligned $[Ca_{1.8}M_{0.2}CoO_3]^{RS}_{0.62}[CoO_2]$($M$=Sr, Y and Bi) and *c*-aligned $[Ca_2Co_{4/3}Cu_{2/3}O_4]^{RS}_{0.62}[CoO_2]$. The dotted lines represent the temperature dependence of the BCS gap energy.

Also, the latest μ^+SR experiment on $[Ca_2Co_{4/3}Cu_{2/3}O_4]^{RS}_{0.62}[CoO_2]$,[13)] which consists of the quadruple rocksalt-type subsystem and the single $[CoO_2]$ subsystem, also indicates the existence of an IC-SDW state below ~200 K. The precession frequency due to an internal IC-SDW field is estimated as ~60 MHz at zero temperature. This strongly suggests that the IC-SDW exists in the $[CoO_2]$ subsystem, because one third of the Co ions in the rocksalt-type subsystem are replaced by Cu ions.[37)] Therefore, the IC-SDW is found to be caused by the spin-order of the conduction electrons in the $[CoO_2]$ subsystem.

3. 3 Other 3-layer cobaltites[22)]

For the cobaltites with triple rocksalt-type subsystem, a new way to control the Co valence was proposed by the analogy of the high-T_c cuprates. That is, the partial substitution of Co in the rocksalt-type subsystem by Ti , Hg, Tl or Pb, as seen in **Table 1**. The systematic change in S suggest that the charge carrier concentration in the CoO_2 planes is successfully controlled in a wider range than the case of $[Ca_{2-z}M_zCoO_3]^{RS}_{x}[CoO_2]$. The crystal structure of these cobaltites is essentially the same as that of $[Ca_2CoO_3]^{RS}_{0.62}[CoO_2]$, *i.e.*, alternating layers of the triple rocksalt-type subsystem and the single CdI_2-type $[CoO_2]$ subsystem stacked along the *c*-axis. There is also a misfit between these two subsystems along the *b*-axis.[16-18)]

Figures 9(a)-(c) show the temperature dependences of A_n, λ_n (n = para and fast) estimated from the wTF-μ^+SR spectrum using Eq. (8) and χ and χ^{-1} in $[Ca_2Pb_{0.4}Co_{0.6}O_3]^{RS}_{0.62}[CoO_2]$. As T decreases from 250 K, the magnitude of A_{para} is nearly independent of temperature down to 150 K, then decreases as T is lowered further. Finally A_{para} seems to level off to a constant value below about 40 K. The decrease in A_{para} below 120 K (and the accompanying increase in λ_{para}) indicate the existence of a magnetic transition with an onset temperature $T_c^{on} = 130 \pm 20$ K, a transition width ΔT ~80 K and an endpoint T_c^{end}~40 K, respectively. Since A_{para} is roughly proportional to the volume of a paramagnetic phase, the volume fraction V_F of the magnetic phase at the lowest temperature measured is estimated to be ~30%.

On the other hand, the $A_{fast}(T)$ curve exhibits a broad maximum at about 50 K, probably due to the onset of even stronger local fields (resulting in unobservably fast muon spin depolarization) below 50 K. Both the $\lambda_{para}(T)$ and the $\lambda_{fast}(T)$ curves exhibit a broad maximum around 80 K. That is, λ_{para} increases with decreasing T from 250 K to 80 K, then decreases below 80 K, and finally levels off to a constant value below 40 K. Meanwhile, λ_{fast} increases with decreasing T from about 120 K (where it is first detected) down to 80 K, after which it decreases down to the lowest temperature measured. It is noteworthy that the highest value of λ_{fast} ($\sim 12\times10^6 s^{-1}$) is 220 times larger than that of λ_{para} ($\sim 0.05\times10^6 s^{-1}$).

Nevertheless, the $\chi(T)$ curve exhibit anomalies neither at T_c^{on} nor at T_c^{end}, although a rapid increase in χ with decreasing T was observed below ~ 20 K (Fig. 9(c)).

This behavior is very similar to the cases of $[Ca_2CoO_3]^{RS}_{0.62}[CoO_2]$ and $[Ca_2Co_{4/3}Cu_{2/3}O_4]^{RS}_{0.62}[CoO_2]$. **Figure 10** shows ZF-μ^+SR time spectra at ~1.8 K for polycrystalline $[Ca_2Pb_{0.4}Co_{0.6}O_3]^{RS}_{0.62}[CoO_2]$, $[Ca_2Ti_{0.4}Co_{0.6}O_3]^{RS}_{0.62}[CoO_2]$, and $[Sr_2Hg_{0.4}Co_{0.6}O_3]^{RS}_{0.56}[CoO_2]$ samples. The top spectrum is reasonably well fitted with Eq. (9) for IC-SDW. Furthermore the IC-SDW frequency is estimated as 59.6 MHz at 1.9 K for $[Pb_{0.4}Co_{0.6}Ca_2O_3]^{RS}_{0.62}[CoO_2]$; this value is very close to that of the other 3- and 4-layer cobaltites (see Fig. 8).

The absence of a clear oscillation in the middle and bottom spectrum indicates an inhomogeneous or a fast fluctuating distribution of internal magnetic fields in the Ti- and Hg-substituted samples, although the origin of the changes in the wTF-μ^+SR spectra below T_c^{on} is considered to be essentially the same as those for the Pb-substituted sample and $[Ca_2CoO_3]^{RS}_{0.62}[CoO_2]$, *i.e.*, the formation of the IC-SDW order.

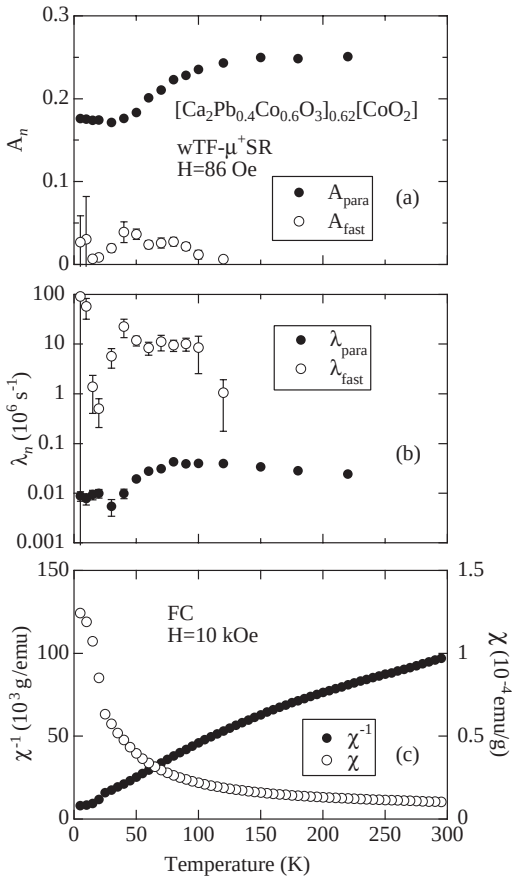

Fig. 9 Temperature dependences of (a) A_{para} and A_{fast} (b) λ_{para} and λ_{fast} and (c) susceptibility (χ) and χ^{-1} in $[Ca_2Pb_{0.4}Co_{0.6}O_3]^{RS}_{0.62}[CoO_2]$. χ was measured with magnetic field H=10 kOe in field cooling mode.

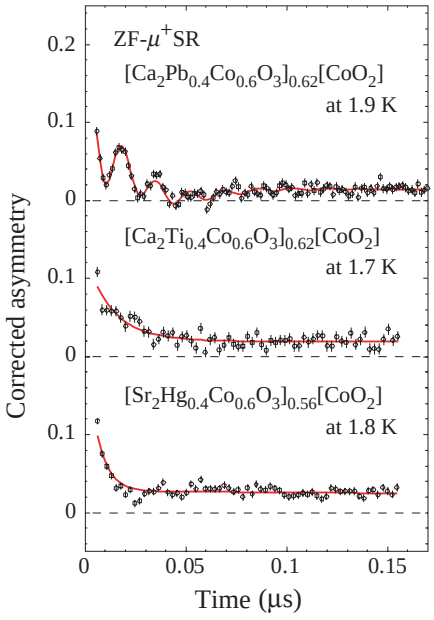

Fig. 10 ZF-μ^+SR time spectra of polycrystalline $[Ca_2Pb_{0.4}Co_{0.6}O_3]^{RS}_{0.62}[CoO_2]$ (top), $[Ca_2Ti_{0.4}Co_{0.6}O_3]^{RS}_{0.62}[CoO_2]$ (middle), and $[Sr_2Hg_{0.4}Co_{0.6}O_3]^{RS}_{0.56}[CoO_2]$ (bottom) samples.

4. Discussion

4. 1 Magnetic phase diagram

For the 3- and 4-layer cobaltites, $[Ca_2CoO_3]^{RS}_{0.62}[CoO_2]$ and $[Ca_2Co_{4/3}Cu_{2/3}O_4]^{RS}_{0.62}[CoO_2]$, the IC-SDW transition was also observed as a common behavior in the CoO_2 planes.[12, 15] We have studied by μ^+SR the dependence of the IC-SDW transition on the Co valence for the variety of layered cobaltites shown in Table 1. It should be noted that the magnetic susceptibility $\chi(T)$ curves for the 3- and 4-layer samples lacked a marked change at either the T_{SDW}^{on} or T_{SDW}^{end} detected by μ^+SR. The volume fraction V_F of the SDW phase in Na_xCoO_2 is smaller than those of the 3- and 4-layer cobaltites, due to the reaction of excess Na with humidity and the resulting disorder in the sandwich layers.[14, 27] Thus, the SDW order is intrinsic, while the other fractions (disorder) are not. Because of the two Co sites in the 3- and 4- layer cobaltite lattices (one in the rocksalt-type subsystem and the other in the CoO_2 plane), it is difficult to determine the Co valence in the CoO_2 plane by χ measurements or chemical titration techniques. Also, a large T dependence of the Hall coefficient of the cobaltites[27] makes difficult to estimate the carrier concentration in the CoO_2 plane. On the other hand, the magnitude of S in the layered cobaltites is almost independent of T above 200 K.[7, 9, 16-18, 37] Therefore, we use the value of S at 300 K as an indicator of the Co valence in the CoO_2 plane for these cobaltites. The modified Heikes formula gives S at the high-temperature limit ($S_{T\to\infty}$) as Ref. 38

$$S_{T\to\infty} = -\frac{k_B}{e}\ln\left(\frac{g_3}{g_4}\frac{y}{1-y}\right), \quad \cdots\cdots\cdots\cdots(10)$$

where k_B is the Boltzmann constant, e is the elementary charge and g_3 and g_4 are the numbers

Table 1 Parameters of the magnetic transition and reported thermopower S of several cobaltites; the number of the layers between the two adjacent $[CoO_2]$ planes (N), the onset and endpoint temperature of the magnetic transition detected by the μ^+SR experiments, the volume fraction of the magnetic phase (V_F) and S at 300 K. nd $\geq$ 3.3 means not detected down to 3.3 K. * and ** indicate the sample showing a clear muon precession due to the IC-SDW (C-SDW) field in a ZF-μ^+SR spectrum. V_F is calculated using the asymmetry of the main oscillating signal in a ZF-μ^+SR spectrum at the lowest temperature measured,whereas for $Na_{0.75}CoO_2$ three oscillating signals were used.[14] † indicates a rough estimation from the wTF-μ^+SR experiments.

cobaltite	N	T_{SDW}^{on} (K)	T_{SDW}^{end} (K)	V_F (%)	S (300 K) (μVK^{-1})
$[Ca_2CoO_3]^{RS}_{0.62}[CoO_2]$	3	100 ± 5	30 ± 5*	84	130
$[Ca_{1.8}Bi_{0.2}CoO_3]^{RS}_{x}[CoO_2]$	3	120 ± 20	70 ± 10*	78	140
$[Ca_{1.8}Y_{0.2}CoO_3]^{RS}_{x}[CoO_2]$	3	120 ± 20	70 ± 10*	92	140
$[Ca_{1.8}Sr_{0.2}CoO_3]^{RS}_{x}[CoO_2]$	3	100 ± 10	45 ± 10*	80	118
$[Ca_2Pb_{0.4}Co_{0.6}O_3]^{RS}_{0.62}[CoO_2]$	3	130 ± 20	40 ± 10*	58	165
$[Sr_1Ca_{0.9}Pb_{0.7}Co_{0.4}O_3]^{RS}_{0.58}[CoO_2]$	3	90 ± 10	10 ± 10	~39 †	130
$[Sr_2Pb_{0.7}Co_{0.3}O_3]^{RS}_{0.56}[CoO_2]$	3	80 ± 10	nd ≥ 3.3	~40 †	120
$[Sr_2Tl_{0.76}Co_{0.33}O_3]^{RS}_{0.56}[CoO_2]$	3	10 ± 40	nd ≥ 5.1	~10 †	90
$[Sr_{1.88}Tl_{1.01}Co_{0.11}O_3]^{RS}_{0.56}[CoO_2]$	3	25 ± 5	nd ≥ 1.7	~18 †	90
$[Sr_{1.78}Tl_{1.18}Co_{0.03}O_3]^{RS}_{0.57}[CoO_2]$	3	nd ≥ 2.5	nd ≥ 2.5	-	90
$[Sr_2Hg_{0.4}Co_{0.6}O_3]^{RS}_{0.56}[CoO_2]$	3	40 ± 25	5 ± 5	~88 †	100
$[Ca_2Ti_{0.4}Co_{0.6}O_3]^{RS}_{0.62}[CoO_2]$	3	150 ± 10	15 ± 5	~92 †	150
$[Ca_2Co_{4/3}Cu_{2/3}O_4]^{RS}_{0.62}[CoO_2]$	4	190 ± 10	145 ± 10*	98	150
$[Ca_2Bi_{1.7}Co_{0.3}O_4]^{RS}_{0.60}[CoO_2]$	4	60 ± 20	nd ≥ 5	~12 †	140
$[Sr_2Bi_2O_4]^{RS}_{x}[CoO_2]$	4	nd ≥ 2.3	nd ≥ 2.3	-	134
$[Ba_2Bi_{1.8}Co_{0.2}O_4]^{RS}_{0.5}[CoO_2]$	4	nd ≥ 1.8	nd ≥ 1.8	-	100
$Na_{0.9}CoO_2$	1	19 ± 0.5	19 ± 3*	50	150
$Na_{0.75}CoO_2$	1	22 ± 0.5	22 ± 1**	21	120
$Na_{0.65}CoO_2$	1	nd ≥ 2.5	nd ≥ 2.5	-	100
$Na_{0.6}CoO_2$	1	nd ≥ 4.3	nd ≥ 4.3	-	100

of the spin configurations of Co^{3+} and Co^{4+}, and y is the ratio $Co^{4+}/(Co^{3+}+ Co^{4+})$. Since both Co^{3+} and Co^{4+} are in the low-spin state and $g_3 = 1$ and $g_4 = 6$, we can convert S (300 K) to y, assuming that $S(300\ \mathrm{K}) = S_{T\to\infty}$.

Figure 11 shows T_{SDW}^{on} as a function of S (300 K) for the all cobaltites listed in Table 1. A clear dome-shaped relation is observed for all the available cobaltites with a variable number of layers (N) between the two adjacent CoO_2 planes. As N increases from 1, the T_{SDW}^{on} -S(300 K) curve shifts towards higher T, due to the increased two-dimensionality induced by the increase in the interlayer distance between CoO_2 planes. Also, the large observed transition widths (50-130 K) are consistent with enhanced two-dimensionality and resulting spin fluctuations. Phenomenologically, the phase diagram is very similar to the well-known relationship between the superconducting T_c and the Cu valence in the high-T_c cuprates. Actually, both SDW and superconducting transitions are induced by an intrinsic instability of an electron system; that is, as T decreases, an energy gap appears at T_{SDW} and/or T_c to minimize the internal energy for both cases. Therefore, it is reasonable to expect a similar relationship between transition temperature and carrier concentration for both the magnetic cobaltites and the superconducting cuprates.

Furthermore, the average Co valence for the maximum T_{SDW} indicates the optimal filling to induce an SDW transition at high T and enhance the effective mass of charge carriers through the AF interaction between spins. In other words, this dome relation provides important guidance in the search for improved thermoelectric properties of the layered cobaltites.

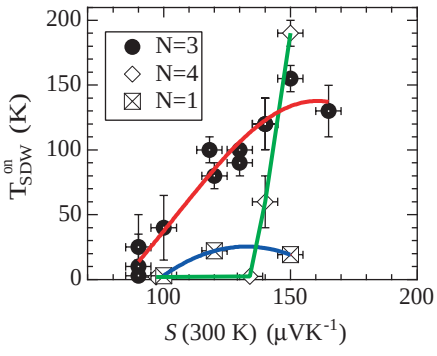

Fig. 11 The relationship between T_{SDW}^{on} and thermopower S at 300 K. Solid circles represent the data for the cobaltites with a triple rocksalt-type subsystem, open diamonds a quadruple rocksalt-type subsystem and crossed squares Na_xCoO_2.

4. 2 Magnitude of internal magnetic field

If the SDW state is induced by the competition between U/t and n in the CoO_2 2DTL, the nature of the SDW state is considered to be essentially same in all the cobaltites. However, the internal magnetic field of the ordered state, f_μ (0 K), is found to be ~3 MHz for Na_xCoO_2, while it is ~60 MHz for $[Ca_2CoO_3]^{RS}_{0.62}[CoO_2]$ and $[Ca_2Co_{4/3}Cu_{2/3}O_4]^{RS}_{0.62}[CoO_2]$.[12, 13, 15] The muon locates probably ~0.1 nm away from the oxygen ions, and there is no space for it in the CoO_6 octahedra in the $[CoO_2]$ plane as in the case for the high-T_c cuprates.[33] This discrepancy is difficult to explain only by differences in the μ^+ site experiencing the SDW field. That is, even if the μ^+s in Na_xCoO_2 locate in the vacant sites in the Na plane and those in the latter two cobaltites are bound to oxygen in the CoO_2 plane, the ratio between the bond length d of Na-Co and O-Co is about 1.65. Assuming that $f_\mu(0\ \mathrm{K}) = 60$ MHz at the oxygen site in the CoO_2 plane, f_μ (0 K) at the Na site would be roughly ~13 MHz, because the dipolar field is pro portional to d^{-3}. This is still four times larger than the experimental result.

Hence, there should be the other reasons for the lower f_μ (0 K) found in Na_xCoO_2. Considering the crystal structure of these cobaltites, the distance between adjacent CoO_2 planes in Na_xCoO_2 is significantly smaller than those in $[Ca_2CoO_3]^{RS}_{0.62}[CoO_2]$ and $[Ca_2Co_{4/3}Cu_{2/3}O_4]^{RS}_{0.62}[CoO_2]$. Thus, the interlayer interaction between the CoO_2 planes in Na_xCoO_2 is considerably larger than in the other layered cobaltites. Such interaction is thought to weaken the two dimensionality of the CoO_2 plane. As a result, the magnitude of f_μ (0 K) in Na_xCoO_2 may be smaller than those in the other layered cobaltites. Indeed, large transition widths, ΔT ~70 K, were observed in $[Ca_2CoO_3]^{RS}_{0.62}[CoO_2]$ and $[Ca_2Co_{4/3}Cu_{2/3}O_4]^{RS}_{0.62}[CoO_2]$, while ΔT ~0 K for Na_xCoO_2. This suggests an increase in spin

frustration, reflecting the decrease in the two-dimensionality in Na_xCoO_2.

5. Summary

In order to elucidate the magnetism in 'good' thermoelectric layer cobaltites, μ^+SR spectroscopy has been used on all known cobaltites at temperatures below 300 K. It was found that a common low temperature magnetic state (which in some cases is manifest as an incommensurate spin density wave IC-SDW) forms in the CoO_2 planes. The magnitude of the transition temperature to the IC-SDW state T_{SDW} is found to be sensitive both to the Co valence in the CoO_2 plane, *i.e.*, the occupancy of the Co spin ($\mathbf{S} = 1/2$) in the triangular lattice, and to the structure of the subsystem sandwiched by the two CoO_2 planes.

A tentative magnetic phase diagram was obtained for Na_xCoO_2 with $x \geq 0.6$. The relationship between T_{SDW} and x changed dome-shaped, as well as the change in the high-T_c cuprates. Since this relationship was explained using the Hubbard model within a mean field approximation for two-dimensional triangular lattice of the CoO_2 plane, which is a common structural component for the all known thermoelectric layered cobaltites, this dome-shaped relationship is concluded to be a common behavior for the layered cobaltites.

Acknowledgements

This work was carried out by the collaboration with Mr. H. Itahara, Dr. T. Tani, Dr. Y. Seno, Mr. K. Dohmae and Dr. C. Xia of Toyota CRDL, Prof. J. H. Brewer of Univ. of British Columbia and Prof. E. J. Ansaldo of TRIUMF. The author appreciate Prof. T. Sasaki, Prof. Y. Mori and Dr. M. Mikami of Osaka Univ., Prof. H. Yamauchi, Prof. M. Karppinen and Dr. T. Motohashi of Tokyo Inst. of Technology, and Dr. A. Maignan and Dr. S. Hébert of Univ. of Caen for providing their samples. The author thank Dr. S. R. Kreitzman, Dr. B. Hitti and Dr. D. J. Arseneau of TRIUMF, Mr. A. Izadi-Najafabadi and Mr. S. D. LaRoy of Univ. of British Columbia for help with the μ^+SR experiments. The author appreciate useful discussions with Dr. R. Asahi of Toyota CRDL, Prof. U. Mizutani, Prof. H. Ikuta and Prof. T. Takeuchi of Nagoya Univ. and Prof. K. Machida of Okayama Univ. This work was supported at Toyota CRDL by joint research and development with International Center for Environmental Technology Transfer in 2002-2004, commissioned by the Ministry of Economy Trade and Industry of Japan, at UBC by the Canadian Inst. for Advanced Research, the Natural Sciences and Engineering Research Council of Canada, and at TRIUMF by the National Research Council of Canada.

References

1) Takada, K., Sakurai, H., Takayama-Muromachi, E., Izumi, F., Dilanian, R. A. and Sasaki, T. : Nature, **422**(2003), 53
2) Schaak, R. E., Klimczuk, T., Foo, M. L. and Cava, R. J. : Nature, **424**(2003), 527
3) Molenda, J., Delmas, C., Dordor, P. and Stoklosa, A. : Solid State Ionics, **12**(1989), 473
4]) Yakabe, H., Kikuchi, K., Terasaki, I., Sasago, Y. and Uchinokura, K. : Proc. 16th Int. Conf. Thermoelecrics, (1997), 523-527, IEEE
5) Terasaki, I., Sasago, Y. and Uchinokura, K. : Phys. Rev. B, **56**(1997), R12685
6) Funahashi, R., Matsubara, I., Ikuta, H., Takeuchi, T., Mizutani, U. and Sodeoka, S. : Jpn. J. Appl. Phys., **39**(2000), L1127
7) Masset, A. C., Michel, C., Maignan, A., Hervieu, M., Toulemonde, O., Studer, F., Raveau, B. and Hejtmanek, J. : Phys. Rev. B, **62**(2000), 166
8) Miyazaki, Y., Kudo, K., Akoshima, M., Ono, Y., Koike, Y. and Kajitani, T. : Jpn. J. Appl. Phys., **39**(2000), L531
9) Tsukada, I., Yamamoto, T., Takagi, M., Tsubone, T., Konno, S. and Uchinokura, K. : J. Phys. Soc. Jpn., **70**(2001), 834
10) Yamamoto, T., Uchinokura, K. and Tsukada, I. : Phys. Rev. B, **65**(2002), 184434
11) Ando, Y., Miyamoto, N., Segawa, K., Kawata, T. and Terasaki, I. : Phys. Rev. B, **60**(1999), 10580
12) Sugiyama, J., Itahara, H., Tani, T., Brewer, J. H. and Ansaldo, E. J. : Phys. Rev. B, **66**(2002), 134413
13) Sugiyama, J., Brewer, J. H., Ansaldo, E. J., Itahara, H., Dohmae, K., Seno, Y., Xia, C. and Tani, T. : Phys. Rev. B, **68**(2003), 134423
14) Sugiyama, J., Itahara, H., Brewer, J. H., Ansaldo, E. J., Motohashi, T., Karppinen, M. and Yamauchi, H. : Phys. Rev. B, **67**(2003), 214420
15) Sugiyama, J., Brewer, J. H., Ansaldo, E. J., Itahara, H., Dohmae, Xia, C., Seno, Y., Hitti, B. and Tani, T. : J. Phys.: Condens. Matter, **15**(2003), 8619
16) Maignan, A., Hébert, S., Pelloquin, D., Michel, C. and Hejtmanek, J. : J. Appl. Phys., **92**(2002), 1964
17) Hébert, S., Lambert, S., Pelloquin, D. and Maignan, A. : Phys. Rev. B, **64**(2001), 172101
18) Pelloquin, D., Maignan, A., Hébert, S., Michel, C. and Raveau, B. : J. Solid State Chem., **170**(2003), 374

19) Krishnamurthy, H. R., Jayaprakash, C., Sarker, S. and Wenzel, W. : Phys. Rev. Lett., **64**(1990), 950
20) Fujita, M., Ichimura, M. and Nakao, K. : J. Phys. Soc. Jpn., **60**(1991), 2831
21) Fujita, M., Nakanishi, T. and Machida, K. : Phys. Rev. B, **45**(1992), 2190
22) Sugiyama, J., Brewer, J. H., Ansaldo, E. J., Itahara, H.,Tani, T., Mikami, M., Mori, Y., Sasaki, T., Hébert, S. and Maignan, A. : Phys. Rev. Lett., **92**(2004), 017602
23) Sugiyama, J., Brewer, J. H., Ansaldo, E. J., Mikami, M., Mori, Y. and Sasaki, T. : Phys. Rev. B, (to be submitted)
24) Kalvius, G. M., Noakes, D. R. and Hartmann, O. : Handbook on the Physics and Chemistry of Rare Earths 32 edited by Gschneidner, Jr. K. A., et al., (2001), 55-451, North-Holland, Amsterdam
25) Brewer, J. H. and Cywinski, R. : Muon Science edited by Lee S. L., et al., (1999), 1-9, Inst. of Phys. Pub., Bristol
26) Luke, G. M., Sternlieb, B. J., Uemura, Y. J., Brewer, J. H., Kadono, R., Kiefl, R. F., Kreitzman, S. R., Riseman, T. M., Gopalakrishnan, J., Sleight, A. W., Subramanian, M. A., Uchida, S., Takagi, H. and Tokura, Y. : Nature, **338**(1989), 49
27) Mikami, M., Yoshimura, M., Mori, Y., Sasaki, T., Funahashi, R. and Shikano, M. : Jpn. J. Appl. Phys., **42**(2003), 7383
28) Motohashi, T., Naujalis, E., Ueda, R., Isawa, K., Karppinen, M. and Yamauchi, H. : Appl. Phys. Lett., **79**(2001), 1480
29) Tani, T., Itahara, H., Xia, C. and Sugiyama, J. : J. Mater. Chem., **13**(2003), 1865
30) Itahara, H., Xia, C., Sugiyama, J. and Tani, T. : J. Mater. Chem., **14**(2004), 61
31) Motohashi, T., Ueda, R., Naujalis, E., Tojo, T., Terasaki, I., Atake, T., Karppinen, M. and Yamauchi, H. : Phys. Rev. B, **67**(2003), 64406
32) Uemura, Y. J. : Muon Science edited by Lee, S. L., et al., (1999), 85-114, Inst. of Phys. Pub., Bristol
33) Grüner, G. : Density Waves in Solids, Chap. 4, (1994), Addison-Wesley-Longmans, Reading
34) Tomeno, I. and Oguchi, M. : J. Phys. Soc. Jpn., **67** (1998), 318
35) Singh, D. J. : Phys. Rev. B, **61**(2000), 13397
36) Sugiyama, J., Xia, C. and Tani, T. : Phys. Rev. B, **67**(2003), 104410
37) Miyazaki, Y., Miura, T., Ono, Y. and Kajitani, T. : Jpn. J. Appl. Phys., **41**(2002), L849
38) Koshibae, W., Tsutsui, K. and Maekawa, S. : Phys. Rev. B, **62**(2000), 6869

(Report received on Jan. 30, 2004)

Jun Sugiyama
Year of birth : 1957
Division : Inorganic Materials Lab.
Research fields : Condensed matter physics
Academic degree : Dr. Eng.
Academic society : Phys. Soc. Jpn., Am. Phys. Soc.